ISSN 1674-1056
http://cpb.iphy.ac.cn
http://iopscience.iop.org/cpb
中国物理 B
Chinese Physics
中国物理 Chinese Physics B

Expansion dynamics of a spherical Bose-Einstein condensate

Rui-Zong Li(李睿宗)[1,3], Tian-You Gao(高天佑)[1], Dong-Fang Zhang(张东方)[1], Shi-Guo Peng(彭世国)[1], Ling-Ran Kong(孔令冉)[1,3], Xing Shen(沈星)[1,3], Kai-Jun Jiang(江开军)[1,2]

Citation: Chin. Phys. B . 2019, 28(10): 106701 . **doi:** 10.1088/1674-1056/ab4177
Journal homepage: http://cpb.iphy.ac.cn; http://iopscience.iop.org/cpb

What follows is a list of articles you may be interested in

Spatiotemporal Bloch states of a spin-orbit coupled Bose-Einstein condensate in an optical lattice

Ya-Wen Wei(魏娅雯), Chao Kong(孔超), Wen-Hua Hai(海文华)
Chin. Phys. B . 2019, 28(5): 056701 . **doi:** 10.1088/1674-1056/28/5/056701

Bloch oscillation of Weyl metal along synthetic dimensions

Ye Xiong(熊烨)
Chin. Phys. B . 2018, 27(12): 126701 . **doi:** 10.1088/1674-1056/27/12/126701

Two types of ground-state bright solitons in a coupled harmonically trapped pseudo-spin polarization Bose–Einstein condensate

T F Xu(徐天赋)
Chin. Phys. B . 2018, 27(1): 016702 . **doi:** 10.1088/1674-1056/27/1/016702

A space-dependent atomic superfluid current in Bose-Einstein condensates

Li Fei, Li Yong-Fan, Zhang Ping-Ke, Ai Zhen-Zhou, Wu Chang-Yi
Chin. Phys. B . 2015, 24(4): 046701 . **doi:** 10.1088/1674-1056/24/4/046701

Production of ^{87}Rb Bose-Einstein condensates in a hybrid trap

Duan Ya-Fan, Jiang Bo-Nan, Sun Jian-Fang, Liu Kang-Kang, Xu Zhen, Wang Yu-Zhu
Chin. Phys. B . 2013, 22(5): 056701 . **doi:** 10.1088/1674-1056/22/5/056701

Expansion dynamics of a spherical Bose–Einstein condensate*

Rui-Zong Li(李睿宗)[1,3], Tian-You Gao(高天佑)[1,†], Dong-Fang Zhang(张东方)[1], Shi-Guo Peng(彭世国)[1], Ling-Ran Kong(孔令冉)[1,3], Xing Shen(沈星)[1,3], and Kai-Jun Jiang(江开军)[1,2,‡]

[1] *State Key Laboratory of Magnetic Resonance and Atomic and Molecular Physics, Wuhan Institute of Physics and Mathematics, Chinese Academy of Sciences, Wuhan* 430071, *China*

[2] *Center for Cold Atom Physics, Chinese Academy of Sciences, Wuhan* 430071, *China*

[3] *School of Physics, University of Chinese Academy of Sciences, Beijing* 100049, *China*

(Received 12 July 2019; revised manuscript received 21 August 2019; published online 30 September 2019)

We experimentally and theoretically observe the expansion behaviors of a spherical Bose–Einstein condensate. A rubidium condensate is produced in an isotropic optical dipole trap with an asphericity of 0.037. We measure the variation of the condensate size in the expansion process after switching off the trap. The free expansion of the condensate is isotropic, which is different from that of the condensate usually produced in the anisotropic trap. We derive an analytic solution of the expansion behavior based on the spherical symmetry, allowing a quantitative comparison with the experimental measurement. The interaction energy of the condensate is gradually converted into the kinetic energy during the expansion and after a long time the kinetic energy saturates at a constant value. We obtain the interaction energy of the condensate in the trap by probing the long-time expansion velocity, which agrees with the theoretical calculation. This work paves a way to explore novel quantum states of ultracold gases with the spherical symmetry.

Keywords: Bose–Einstein condensate, spherical trap, free expansion

PACS: 67.85.–d, 67.10.Ba, 34.50.Cx, 37.10.De **DOI:** 10.1088/1674-1056/ab4177

1. Introduction

In the ultracold Bose–Einstein condensate (BEC), the interatomic interaction modifies the system behaviors to deviate from the ideal gas,[1] which provides a platform to explore exotic quantum phenomena such as low-energy excitations,[2–4] phase transitions in optical lattices,[5–7] artificial gauge potential,[8,9] low-dimension physics,[10,11] and many others. Due to the small *in-situ* size of the condensate in the trap, the cold atomic sample is usually probed after certain free expansion time.[12] The interatomic interaction plays an important role to determine the expansion dynamics. After the condensate being released from the trap, the interaction energy is converted to the kinetic energy and the initial acceleration after switching off the trap is determined by the gradient of the interaction energy.[13–15] The expansion behaviors of the condensate are dependent on the shape of the external trap, namely, the initial condition of the system. Previously the condensate is mostly produced in an anistotropic trap (i.e., $\varepsilon \neq 1$, where ε is the aspect ratio between the axial and radial frequencies) due to the technical challenge, which leads to an increased degree of complexity in the study of the free expansion. In this case, the expansion behaviors could not be analytically solved without approximation because solving different coupled second-order differential equations is required.[1,15–17] Obtaining the quantum system with an analytic solution allows a more lucid description of the condensate dynamics and an immediate comparison between experiment and theory. Condensate in an isotropic trap (i.e., $\varepsilon = 1$) is a special case that the expansion behavior can be analytically solved. Here we only need to solve one differential equation due to the spherical symmetry. Nevertheless, the experimental study of this expansion is still lacking.

Previously, Hodby *et al.* were able to modify the aspect ratio ($\varepsilon = 2.83$–1.6) in a magnetic trap while keeping the confinement tight.[18] However they did not report achieving a fully isotropic trap. Lobser and his colleagues realized an isotropic magnetic trap with the aid of the gravity force.[19] But the weak confinement (the trapping frequency $\omega \approx 2\pi \times 9$ Hz) in their work is disadvantageous to obtain a pure condensate.

In this paper, we produce a spherical rubidium condensate in an optical dipole trap with an asphericity of 0.037. The large trapping frequency ($2\pi \times 77.5$ Hz) is favorite to produce a pure condensate. Then we measure the condensate widths in the expansion process as well as the interaction energy of the condensate in the trap. We find that the condensate expansion is isotropic and the experimental results agree well with the analytic solution based on the spherical symmetry, which are different from our previous study[20] and other group's works[1,21–23] on the non-spherical BEC. We explore the expansion dynamics in which the the interaction energy is grad-

*Project supported by the National Key Research and Development Program of China (Grant No. 2016YFA0301503), the National Natural Science Foundation of China (Grant Nos. 11674358, 11434015, and 11474315), and Chinese Academy of Sciences (Grant No. YJKYYQ20170025).

†Corresponding author. E-mail: 602gty@sina.com

‡Corresponding author. E-mail: kjjiang@wipm.ac.cn

© 2019 Chinese Physical Society and IOP Publishing Ltd

ually converted into the kinetic energy and after a long time the expansion velocity reaches a constant value.

The paper is organized as follows. We first present the production of a spherical rubidium condensate in Section 2. Then we introduce the expansion behaviors of the condensate in Section 3. Subsequently the interaction energy of the condensate in the trap is obtained in Section 4. Finally, the conclusions are summarized in Section 5.

2. Production of a spherical Bose condensate

The experimental setup is composed of double magneto-optical traps (MOTs), which is similar to that in our previous works.[20,24,25] ^{87}Rb atoms are cooled and trapped in the first MOT and then transferred to the second MOT with a series of optical pushing pulses. In the second MOT, the atom number is $8.5(9)\times10^8$ and the temperature is 320(40) μK. The atom temperature is further reduced to 130(20) μK after a sub-Doppler cooling process. Then the atoms are loaded into a magnetic trap, where the atom number is $2.0(7)\times10^8$ and the temperature is 210(25) μK. Subsequently the atoms are cooled with the radio frequency (RF) induced evaporation cooling to 15(3) μK and then transferred into a hybrid trap composed of magnetic and optical dipole fields.[16] Finally we transfer the cold atoms into an optical dipole trap by gradually switching off the magnetic trap.

We produce a spherical ^{87}Rb BEC in an optical dipole trap in which the trapping frequencies along x, y, z directions are the same. As shown in Fig. 1(a), the optical dipole trap is composed of two far red-detuned laser beams with the wavelength $\lambda = 1064$ nm. The Rayleigh length, $z_R = \pi w_0^2/\lambda$, is much longer than the beam waist w_0. For a single laser beam, the trapping frequency in the radial direction is about 200 times larger than that in the axial direction. So the trapping effect along the propagation direction can be neglected. To produce a fully isotropic trap, the gravity force should be included.[18,19] The trapping potential, which is composed of the optical dipole trap and the gravity, is given by

$$U(x,y,z) = -U_1\exp\left(-\frac{2x^2}{w_{1x}^2}-\frac{2z^2}{w_{1z}^2}\right) - U_2\exp\left(-\frac{2y^2}{w_{2y}^2}-\frac{2z^2}{w_{2z}^2}\right) - mgz, \quad (1)$$

where w_{1x} (w_{2y}) and w_{1z} (w_{2z}) are the waists of the optical beam propagating along the y (x) direction, and U_1 and U_2 are the peak potential energies of the two beams, respectively. By expanding Eq. (1) in the potential minimum $(0,0,z_0)$ to the second order, forming a spherical BEC should satisfy the conditions

$$U_1 = \frac{mgw_{1x}^2}{2a}\sqrt{\frac{w_{1x}^2/w_{1z}^4 + w_{2y}^2/w_{2z}^4}{a-1}}, \quad (2)$$

$$U_2 = \frac{mgw_{2y}^2}{2a}\sqrt{\frac{w_{1x}^2/w_{1z}^4 + w_{2y}^2/w_{2z}^4}{a-1}}, \quad (3)$$

where $a = w_{1x}^2/w_{1z}^2 + w_{2y}^2/w_{2z}^2$. In the experiment, we can accurately adjust the intensities of the two beams to simultaneously match Eqs. (2) and (3).

Now we can discuss the solutions of Eqs. (2) and (3) for a spherical trap. (i) If the confinement in the vertical direction is stronger than that in the horizontal direction for the optical dipole trap (i.e., $a > 1$), it can be weakened by the gravity sag so that the trapping frequencies along x, y, z directions can be identical. In this condition, there exists a solution for Eqs. (2) and (3). (ii) If the confinement in the vertical direction is equivalent to or weaker than that in the horizontal direction (i.e., $a \leq 1$), the trapping frequency in the vertical direction is always smaller than that in the horizontal direction under the gravity sag. In this condition, there is no solution. (iii) If neglecting the gravity term in Eq. (1) (for example, the gravity is compensated by an appropriate gradient magnetic field), the condition of forming a spherical trap will change to the equation $a = w_{1x}^2/w_{1z}^2 + w_{2y}^2/w_{2z}^2 = 1$. But it is a big technical challenge to accurately satisfy this equation by adjusting the relative shapes of the two laser beams. So in our experiment, we choose the condition $a > 1$ to form a spherical trap.

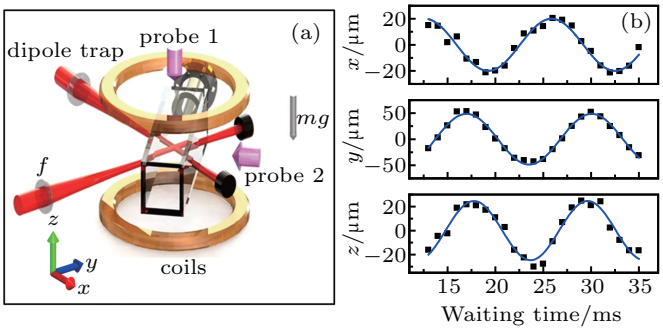

Fig. 1. (a) Experimental setup. The optical dipole trap is composed of two focused red-detuned laser beams in x and y directions. The gravity is in $-z$ direction. Ultracold atoms are simultaneously probed in the vertical and horizontal directions. (b) Measuring the trapping frequencies by probing the oscillations of the centers of mass along three directions respectively. Each experimental data is the average of three measurements. The solid line is the fitting with a sinusoidal wavefunction.

We measure the trapping frequency by probing the center-of-mass (COM) motion of the atomic cloud in the trap. After displacing atoms away from the equilibrium position for 2 ms, the COMs of the atomic cloud along x, y, and z directions are monitored, respectively. The experimental results are shown in Fig. 1(b). Using a sinusoidal wavefunction $r_i = A_i\sin(\omega_i t + \phi_i)$ ($i = x,y,z$ and $r_i \to i$) to fit the experimental data, we get the trapping frequencies $\omega_x = 2\pi\times76.7(14)$ Hz, $\omega_y = 2\pi\times76.5(6)$ Hz, and $\omega_z = 2\pi\times79.4(12)$ Hz. The frequency uncertainties are from the fitting process. The mean trapping frequency ($\bar{\omega} = (\omega_x+\omega_y+\omega_z)/3 = 2\pi\times77.5$ Hz) is much larger than that in Ref. [19]. The asphericity $A =$

$(\omega_{\max}-\omega_{\min})/\bar{\omega}\approx 0.037$, where $\omega_{\max}$ and $\omega_{\min}$ are the maximum and minimum trapping frequencies along the three directions, respectively. The tight confinement here is favorite to produce a pure condensate with negligible thermal gases and obtain experimental data with a large signal-to-noise ratio. We improve the position stability of the optical trap beam to be better than 3 μm, keeping the condensate well in a spherical shape. The atoms stay in the spin state $|F,m_F\rangle=|1,-1\rangle$. The atom number is $1.2(2)\times 10^5$ and the temperature is 80(5) nK. The BEC is well in the hydrodynamic limit with an adimensional parameter $Na_s/a_{ho}\approx 570\gg 1$,[27] where a_s is the s-wave scattering length, $a_{ho}=\sqrt{\hbar/m\omega}$ is the harmonic oscillator length of the trap, and N is the atom number.

It should be noted that one limitation of the optical trap is the anharmonicity, which is specially serious for a big condensate. Fortunately, the atomic cloud in the trap is small ($R\approx 7.3$ μm) due to the large trapping frequency in our experiment, greatly softening the anharmonicity. The small anharmonicity does not affect the key features of the experimental results.

After suddenly switching off the optical trap, we measure the aspect ratio $\eta(t)$ of the condensate during the free expansion. The experimental results are shown in Fig. 2. The condensate width $R_i(t)$ during the expansion is obtained by fitting the optical density of the image with a Thomas–Fermi (TF) distribution. For the images probed in the horizontal direction, $\eta(t)=R_{\parallel}(t)/R_z(t)$, where $R_{\parallel}(t)$ and $R_z(t)$ are the TF radii in the horizontal and vertical directions, respectively. For the images probed in the vertical direction, $\eta(t)=R_x(t)/R_y(t)$, where $R_x(t)$ and $R_y(t)$ are the TF radii in the x and y directions, respectively. $\eta(t)$ remains unity during the free expansion, which is unique for a spherical BEC. For an non-spherical BEC, the expansion is anisotropic and the aspect ratio $\eta(t)$ approaches an asymptotic value dependent on the ratio of the trapping frequencies.[1,15,21–23]

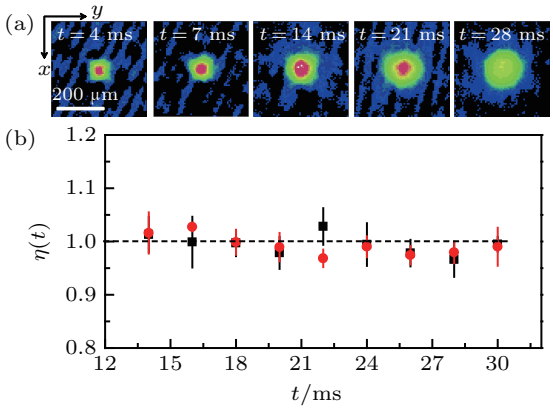

Fig. 2. Isotropic expansion of the condensate. (a) Exemplary images probed in the vertical direction for five expansion times. (b) The aspect ratio $\eta(t)$ versus the expansion time t. The black squares (red circles) are for the images probed in the horizontal (vertical) direction. Each error bar indicates the uncertainty of three measurements. The dashed line denotes the value of unity.

3. Expansion behavior of the condensate

Interatomic interaction plays an important role to determine the expansion dynamics of BEC. Figure 3(a) briefly indicates variations of different energy components in the expansion process.[1,13,16] The chemical potential $\mu=E_{\rm kin}+E_{\rm p}+2E_{\rm int}$ is composed of kinetic energy $E_{\rm kin}$, potential energy $E_{\rm p}$, and interaction energy $E_{\rm int}$. In the trap, $E_{\rm kin}$ is negligibly small and $E_{\rm p}=1.5E_{\rm int}$ according to the Virial relation $2E_{\rm kin}-2E_{\rm p}+3E_{\rm int}=0$. After BEC being released from the trap, $E_{\rm p}$ is switched off and $E_{\rm int}$ starts to be converted into $E_{\rm kin}$ gradually, which makes the release energy $E_{\rm rel}=E_{\rm kin}+E_{\rm int}$ keep constant during the expansion. After a long-time expansion, the interaction energy is completely converted to the kinetic energy. This provides a efficient way to measure the interaction energy of BEC in the trap by probing the long-time expansion velocity, which will be followed in Section 4.

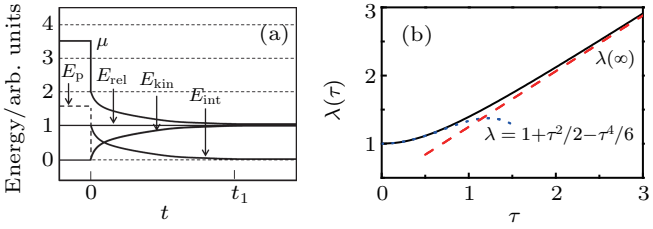

Fig. 3. (a) Schematics of energy components during the free expansion. The trapping potential is switched off at $t=0$. $E_{\rm p}$ is the potential energy, $E_{\rm rel}$ is the release energy, $E_{\rm kin}$ is the kinetic energy, $E_{\rm int}$ is the interaction energy, and μ is the chemical potential. After a long-time expansion ($t>t_1$), the interaction energy is completely converted to the kinetic energy. (b) The scaling factor $\lambda(\tau)=R(\tau)/R(0)$ versus the scaling expansion time τ. $R(0)$ is the TF radius of the BEC in the trap and $\tau=\omega t$. The black solid curve denotes the calculation with Eq. (5) for the whole expansion process. The blue dotted curve indicates the calculation with Eq. (6) for the short-time expansion. The red dashed curve is the calculation with Eq. (7) for the long-time expansion.

During the expansion, the atomic cloud experiences just a free dilatation. Three scaling factors, i.e., $\lambda_i(t)\equiv r_i(t)/r_i(0)$ $(i=x,y,z)$, may be introduced as in Refs. [1], [15], [21], and [22] which describe the trajectory of any infinitesimally small fraction at the position $\boldsymbol{r}(t)$ of the moving cloud. For an axially symmetric BEC (i.e., $\lambda_x(t)=\lambda_y(t)\neq\lambda_z(t)$) mostly produced previously, it is required to solve two coupled second-order differential equations to get the evolution of the scaling factors,[1,15–17] where the analytic solution is generally absent. While for a spherical BEC with $\lambda(t)=\lambda_x(t)=\lambda_y(t)=\lambda_z(t)$, the two coupled differential equations simply merge into one

$$\frac{\partial^2\lambda}{\partial\tau^2}=\lambda^{-4}. \tag{4}$$

The solution can be obtained analytically as

$$\tau=-\sqrt{\frac{3}{2}}\cdot\frac{\sqrt{\pi}\Gamma(2/3)}{\Gamma(1/6)}+\sqrt{\frac{3}{2}}\lambda\cdot{}_2\mathrm{F}_1\left(-\frac{1}{3},\frac{1}{2},\frac{2}{3},\frac{1}{\lambda^3}\right), \tag{5}$$

where $\tau=\omega t$, $\Gamma(\cdot)$ is the Gamma function, and ${}_2\mathrm{F}_1(a,b,c,z)$ is the hypergeometric function.

According to Eq. (5), we can easily obtain the asymptotic behavior of the scaling factor $\lambda(\tau)$ for a short- or long-time expansion

$$\lambda(\tau) \approx 1+\tau^2/2-\tau^4/6, \quad (\tau \to 0), \tag{6}$$

$$\lambda(\tau) \approx \sqrt{2/3}\tau+\frac{\sqrt{\pi}\Gamma(2/3)}{\Gamma(1/6)}, \quad (\tau \to \infty). \tag{7}$$

The scaling factor of the condensate in the expansion process is shown in Fig. 3(b). For the short-time expansion ($\tau \to 0$), $\partial\lambda/\partial\tau \approx \tau$ and $\partial^2\lambda/\partial\tau^2 \approx 1-2\tau^2$. This means that after the trap being switched off, the expansion is speeding and the acceleration decreases versus the expansion time. These behaviors can be understood that the interaction energy is gradually converted into the kinetic energy and decreases during the expansion.[1,16,23] For the long-time expansion ($\tau \to \infty$), $\partial\lambda/\partial\tau \approx \sqrt{2/3}$. In this region, the interaction energy has been completely converted to the kinetic energy and the expansion velocity finally reaches a constant value. The intermediate region with $\tau \approx 1$ indicates the crossover from the acceleration regime to the linear expansion. The quantitative calculations in Fig. 3(b) provide a lucid description of the expansion dynamics. Under the TF approximation, the complete conversion time of the interaction energy into kinetic energy is roughly determined by the trapping frequency ($t \approx 1/\omega$) and has no dependence on the scattering length. The effect of the scattering length is included in the initial density distribution of the condensate.

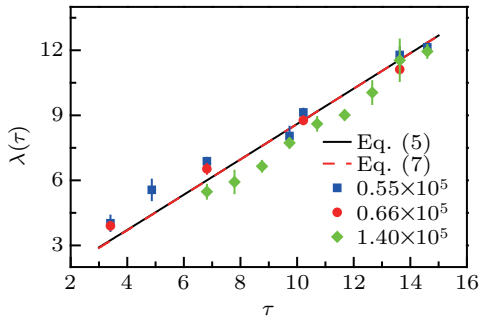

Fig. 4. Scaling factor $\lambda(\tau)$ in the long-time expansion. The black solid curve is the calculation with Eq. (5). The red dashed curve is the calculation with Eq. (7) for the long-time expansion. Blue squares, red circles, and green diamonds denote the measurements with atom numbers of 0.55×10^5, 0.66×10^5, and 1.40×10^5, respectively. Each error bar is the uncertainty of three measurements.

In Fig. 4, we measure the scaling factor during the expansion. The size of the cloud is defined as $R(\tau) = [R_x(\tau)+R_y(\tau)+R_z(\tau)]/3$, where $R_i(\tau)$ $(i=x,y,z)$ is the TF radius of the condensate, and $\lambda(\tau) = R(\tau)/R(0)$. Under the TF approximation, $R(0)$ is calculated from the atom number and trapping frequency, and $R(\tau)$ is measured in the experiment. The experimental results with three atomic numbers are consistent with the theoretical prediction of Eq. (5). Due to the limited resolution of the imaging system ($\Delta r \approx 7.6$ μm),[25] we show the experimental data for expansion time larger than 7 ms (i.e., $\tau > 3.4$). In this region, the interaction energy of the condensate has been completely converted to the kinetic energy. So our current experimental results only demonstrate the long-time expansion behavior as predicted with Eq. (7). In order to observe the short-time expansion with $\tau \leq 1$, an imaging system with a larger numerical aperture is required.

4. Interaction energy of the condensate

During the expansion, the interaction energy is gradually converted into the kinetic energy $E_{\rm kin}$. After atoms being releasing from the trap, $E_{\rm kin}$ can be written in the following integral:

$$E_{\rm kin} = \int \frac{1}{2}m\left[\frac{{\rm d}\boldsymbol{r}(t)}{{\rm d}t}\right]^2 n[\boldsymbol{r}(t)]\,\mathcal{D}[\boldsymbol{r}(t)], \tag{8}$$

where $n[\boldsymbol{r}(t)]$ is the density at position $\boldsymbol{r}(t)$, and m is the atomic mass. By using $\boldsymbol{r}(t) = \lambda(t)\boldsymbol{r}(0)$, equation (8) becomes

$$E_{\rm kin} = \frac{1}{2}m\left[\frac{{\rm d}\lambda(t)/{\rm d}t}{\lambda(t)}\right]^2 \int \boldsymbol{r}(t)^2 n[\boldsymbol{r}(t)]\,\mathcal{D}[\boldsymbol{r}(t)]. \tag{9}$$

It was shown in Ref. [15] that the density $n(\boldsymbol{r})$ still satisfies the generalized TF distribution for a time-dependent problem, which takes the form

$$n[\boldsymbol{r}(t)] = \frac{15}{8\pi R(t)^3}\left[1-\frac{r(t)^2}{R(t)^2}\right], \tag{10}$$

for a spherical atomic cloud, where $R(t)$ is the generalized TF radius at the time t, $n[\boldsymbol{r}(t)]$ has been normalized to unity, i.e., $\int_{\mathcal{S}} n[\boldsymbol{r}(t)]\,\mathcal{D}[\boldsymbol{r}(t)] = 1$, and $\mathcal{S}$ is a spherical domain with radius $R(t)$. Substituting Eq. (10) into Eq. (9), we easily obtain

$$E_{\rm kin} = \frac{1}{2}m\cdot\frac{3}{7}\left[\frac{{\rm d}R(t)}{{\rm d}t}\right]^2. \tag{11}$$

As shown in Fig. 3, the interaction energy is completely converted to the kinetic energy after a long-time expansion. So the interaction energy $E_{\rm int}$ at $t \to 0$ is roughly equivalent to the kinetic energy $E_{\rm kin}$ at $t \to \infty$.

We can check the validity of Eq. (11). From Eq. (7), the size of the cloud $R(t)$ at $t \to \infty$ should behave as

$$R(t) \approx \sqrt{\frac{2}{3}}\omega t R(0), \tag{12}$$

where $R(0)$ is the size at $t = 0$. Then the interaction energy of the condensate in the trap becomes

$$E_{\rm int} = \frac{1}{2}m\cdot\frac{3}{7}\cdot\frac{2}{3}\omega^2 R(0)^2 = \frac{2}{7}\mu, \tag{13}$$

where $\mu = m\omega^2 R(0)^2/2$ is the chemical potential in the trap. Equation (13) is consistent with the well-known result $E_{\rm int} = 2\mu/7$.[1]

In the experiment, we extract the expansion velocity for the long-time expansion by linearly fitting the TF radii of the condensate. One example of this fitting process is shown in

the inset of Fig. 5. The expansion time is long with $t > 14$ ms (i.e., $\tau > 6.8$), which ensures that the expansion velocity has approached the constant value (see Fig. 3(b)). Then the interaction energy of the condensate in the trap can be calculated with Eq. (11).

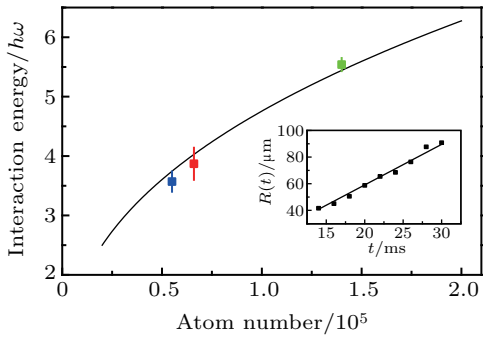

Fig. 5. Interaction energy of the condensate in the trap versus the atom number. The solid curve is the theoretical calculation with Eq. (14). The measurements are for atom numbers of 0.55×10^5, 0.66×10^5, and 1.40×10^5. The error bar is the uncertainty in fitting the expansion velocity. The inset shows an example for linearly fitting the measured TF radii of the condensate with the atom number of 1.40×10^5.

On the other hand, the chemical potential of the condensate in the trap can be calculated with[1,13–15]

$$\mu = \frac{\hbar\omega}{2}\left(\frac{15Na_{\rm s}}{a_{\rm ho}}\right)^{2/5}. \tag{14}$$

The interaction energy of the condensate in the trap versus the atom number is ploted in Fig. 5. The experimental measurements are consistent with the theoretical prediction with Eq. (14).

5. Conclusion and prospect

In conclusion, we experimentally observe the expansion behaviors of a spherical Bose condensate. A spherical rubidium condensate is produced in an optical dipole trap and the characteristic isotropic expansion is observed in the experiment. The condensate widths in the expansion process as well as the interaction energy of the condensate in the trap are measured. We find that the expansion in the short time is speeding and then after a long time the expansion velocity reaches a constant value. The intrinsic mechanics of this behavior is that the interaction energy is converted into the kinetic energy at the beginning of the expansion and the kinetic energy saturates after a long-time expansion. All the measurements agree well with the analytic solution based on the spherical symmetry.

The spherical condensate has unique features due to the spherical symmetry, which paves the way of our future research. First, we will study the exotic quantum state in the spin–orbital–angular-momentum (SOAM) coupled condensate in which the rotation symmetry is required.[24,28,29] Secondly, the excitation spectrum of the condensate is simplified by degeneracy.[1,27,30] The well-defined symmetry facilitates the studies of coupling between collective modes and their Landau damping rates.[31] Quantitative calculations of these processes currently have been carried out.[30,32–34] We will accurately measure the collective mode of the spherical condensate in the finite-temperature regime, extracting subtle many-body effects like thermal and quantum fluctuations.[35–38] In addition, compared to a magnetic trap, the spherical trap composed of the optical field is advantageous to study the non-equilibrium dynamics, where fast modulation of the confinement strength is generally applied.

References

[1] Dalfovo F, Giorgini S, Pitaevskii L P and Stringari S 1999 *Rev. Mod. Phys.* **71** 463
[2] Jin D S, Ensher J R, Matthews M R, Wieman C E and Cornell E A 1996 *Phys. Rev. Lett.* **77** 420
[3] Mewes M-O, Andrews M R, van Druten N J, Kurn D M, Durfee D S, Townsend C G and Ketterle W 1996 *Phys. Rev. Lett.* **77** 988
[4] Ozeri R, Katz N, Steinhauer J and Davidson N 2005 *Rev. Mod. Phys.* **77** 187
[5] Bloch I, Dalibard J and Zwerger W 2008 *Rev. Mod. Phys.* **80** 885
[6] Georgescu I M, Ashhab S and Nori F 2014 *Rev. Mod. Phys.* **86** 153
[7] Eckardt A 2017 *Rev. Mod. Phys.* **89** 011004
[8] Lin Y J, Jimenez-Garcia K and Spielman I B 2011 *Nature* **471** 83
[9] Dalibard J, Gerbier F, Juzeliūnas G and Öhberg P 2011 *Rev. Mod. Phys.* **83** 1523
[10] Kinoshita T, Wenger T and Weiss D S 2006 *Nature* **440** 900
[11] Cazalilla M A, Citro R, Giamarchi T, Orignac E and Rigol M 2011 *Rev. Mod. Phys.* **83** 1405
[12] Ketterle W, Durfee D and Stamper-Kurn D 1999 *In Bose-Einstein condensation in atomic gases, Proceedings of the International School of Physics "Enrico Fermi", Course CXL (M Inguscio, S Stringari and C E Wieman* (IOS Press: Amsterdam) pp. 67–176
[13] Dalfovo F and Stringari S 1996 *Phys. Rev. A* **53** 2477
[14] Baym G and Pethick C J 1996 *Phys. Rev. Lett.* **76** 6
[15] Castin Y and Dum R 1996 *Phys. Rev. Lett.* **77** 5315
[16] Holland M J, Jin D S, Chiofalo M L and Cooper J 1997 *Phys. Rev. Lett.* **78** 3801
[17] Dalfovo F, Minniti C, Stringari S and Pitaevskii L P 1997 *Phys. Lett. A* **227** 259
[18] Hodby E, Hechenblaikner G, Marago O M, Arlt J, Hopkins S and Foot C J 2000 *J. Phys. B: At. Mol. Opt. Phys.* **33** 4087
[19] Lobser D S, Barentine A E S, Cornell E A and Lewandowski H J 2015 *Nat. Phys.* **11** 1009
[20] Zhang D, Gao T, Kong L, Li K and Jiang K 2016 *Chin. Phys. Lett.* **33** 76701
[21] Ernst U, Marte A, Schreck F, Schuster J and Rempe G 1998 *Europhys. Lett.* **4** 1
[22] Ernst U, Schuster J, Schreck F, Marte A, Kuhn A and Rempe G. 1998 *Appl. Phys. B* **67** 719
[23] Mewes M-O, Andrews M R, van Druten N J, Kurn D M, Durfee D S and Ketterle W 1996 *Phys. Rev. Lett.* **77** 416
[24] Zhang D, Gao T, Zou P, Kong L, Li R, Shen X, Chen X, Peng S, Zhan M, Pu H and Jiang K 2019 *Phys. Rev. Lett.* **122** 110402
[25] Gao T, Zhang D, Kong L, Li R and Jiang K 2018 *Chin. Phys. Lett.* **35** 86701
[26] Lin Y J, Perry A R, Compton R L, Spielman I B and Porto J V 2009 *Phys. Rev. A* **79** 063631
[27] Stringari S 1996 *Phys. Rev. Lett.* **77** 2360
[28] Chen H R, Lin K Y, Chen P K, Chiu N C, Wang J B, Chen C A, Huang P P, Yip S K, Kawaguchi Y and Lin Y J 2018 *Phys. Rev. Lett.* **121** 113204
[29] Chen P K, Liu L R, Tsai M J, Chiu N C, Kawaguchi Y, Yip S K, Chang M S and Lin Y J 2018 *Phys. Rev. Lett.* **121** 250401
[30] Guilleumas M and Pitaevskii L P 1999 *Phys. Rev. A* **61** 013602
[31] Gao T, Pan J S, Zhang D, Kong L, Li R, Shen X,Chen X, Peng S G,Zhan M, Liu W V and Jiang K 2018 *arXiv: 1805.04727*
[32] Pitaevskii L 1997 *Phys. Lett. A* **229** 406
[33] Rusch M, Morgan S A, Hutchinson D A W and Burnett K 2000 *Phys. Rev. Lett.* **85** 4844
[34] Straatsma C J E, Colussi V E, Davis M J, Lobser D S, Holland M J, Anderson D Z, Lewandowski H J and Cornell E A 2016 *Phys. Rev. A* **94** 043640
[35] Liu X J, Hu H, Minguzzi A and Tosi M P 2004 *Phys. Rev. A* **69** 043605
[36] Williams J E and Griffin A 2001 *Phys. Rev. A* **64** 013606
[37] Jackson B and Zaremba E 2002 *Phys. Rev. A* **66** 033606
[38] Giorgini S 2000 *Phys. Rev. A* **61** 063615